

Glyoxylic-Acetal-Based Gel-Polymer Electrolytes for Lithium-Ion Batteries

Christian Leibing,^[a, b] Simon Muench,^[b, c] Juan Luis Gómez Urbano,^[a, b] Ulrich S. Schubert,^[b, c] and Andrea Balducci^{*[a, b]}

This work focuses on the combination of two strategies to improve the safety of lithium-ion batteries: The use of a glyoxylic-acetal, 1,1,2,2-tetraethoxyethane, in the solvent blend to reduce the flammability of the liquid electrolyte and further its confinement inside of a methacrylate-based polymer matrix, to prevent electrolyte leakage from the battery cells. Physico-chemical characterizations of this novel gel-polymer electrolyte (GPE) confirm its improved thermal properties and suitable ionic conductivity, as well as electrochemical stability window. Tests

in LFP and hard carbon half-cells vs. lithium metal show that the combination of glyoxylic-acetal-based electrolyte and the methacrylate-based polymer matrix can promote lithium-ion intercalation and deintercalation with stable capacity values. The application in lithium-ion battery full cells furthermore shows that the GPE can promote a similar performance compared to the respective liquid electrolyte and can therefore make possible the realization of energy storage devices with improved safety characteristics.

Introduction

Although being widely considered as a “mature” technology, the interest in further improving lithium-ion batteries (LIB) in multiple aspects continues to grow, based on the annual number of publications.^[1,2] So far, research efforts focus on improving the energy density or cycle life by modifications on the insertion electrode materials or by considering alternative LIB concepts like the use of lithium metal as negative electrode.^[3] However, the massive implementation of LIBs in the transport sector has also placed attention on safety aspects and tolerance of extreme conditions (i.e. high voltage, temperature).^[4,5] A key role in this regard comes to the electrolyte, traditionally consisting of a lithium salt dissolved in a mixture of organic carbonate solvents, it represents a highly flammable component of the battery with a risk of leakage.^[6] The established way of addressing the safety characteristics of the lithium-ion battery cell via the electrolytes currently involves the utilization of additives, such as overcharge inhibitors or flame retardants.^[7] However, another suitable

strategy is to replace the most flammable components of conventional electrolytes, which generally are linear carbonates like dimethyl carbonate (DMC), diethyl carbonate (DEC), or ethyl methyl carbonate (EMC). In this regard, great efforts have been made to find promising candidates not only from a safety point of view but also with respect to their sustainability (e.g. fluorine-free electrolyte formulations, bio-based solvents).^[8–11] Nevertheless, most of them cannot individually meet all requirements for proper LIBs operation, such as generating a stable solid electrolyte interphase (SEI) or providing sufficient transport properties at room temperature. Among them, the family of glyoxylic-acetals stands out as an exception for the suitable replacement of flammable linear carbonates. One prominent example is 1,1,2,2-tetraethoxyethane (tetraethoxyglyoxal, TEG), an inexpensive, non-toxic solvent that is industrially used in the fabrication of paints and varnishes.^[12] It offers an elevated flash point of 71 °C along with a low melting point of –35 °C and a good solubilization ability for a broad range of salts.^[13] Previous works demonstrated the applicability of this solvent in lithium, sodium, and potassium-ion batteries and underlined its advantages regarding SEI formation, cycling stability, and performance at elevated temperatures.^[14–18] Accelerating reaction calorimetry measurements conducted by Atik et al. proved that replacing linear carbonates like EMC with TEG effectively increases the onset temperature of a thermal runaway of lithium-ion battery cells.^[19] The combination of TEG with PC as co-solvent and LiTFSI as conductive salt demonstrated a well-balanced combination of transport and thermal properties, displaying also a good cycling stability when evaluated in LIBs.^[20]

Even though, energy storage devices containing liquid electrolytes are still suspect to a risk of leakage that may occur by perforation of the cell. To avoid electrolyte losses, one of the most promising strategies is to utilize ceramic or polymer solid electrolytes. However, they generally suffer from insufficient ionic conductivity or high interfacial resistance, reducing the

[a] C. Leibing, J. L. Gómez Urbano, A. Balducci
Institute for Technical Chemistry and Environmental Chemistry, Friedrich Schiller University Jena, Philosophenweg 7a, 07743, Jena, Germany
E-mail: andrea.balducci@uni-jena.de

[b] C. Leibing, S. Muench, J. L. Gómez Urbano, U. S. Schubert, A. Balducci
Center for Energy and Environmental Chemistry Jena (CEEC Jena)
Philosophenweg 7a, 07743, Jena, Germany

[c] S. Muench, U. S. Schubert
Institute for Organic and Macromolecular Chemistry (IOMC), Friedrich Schiller University Jena, Humboldtstr. 10, 07743, Jena, Germany

 Supporting information for this article is available on the WWW under <https://doi.org/10.1002/batt.202400453>

 © 2024 The Authors. *Batteries & Supercaps* published by Wiley-VCH GmbH. This is an open access article under the terms of the Creative Commons Attribution Non-Commercial License, which permits use, distribution and reproduction in any medium, provided the original work is properly cited and is not used for commercial purposes.

rate performance of the cell.^[6] Thus, the use of a polymeric quasi-solid matrix for the encapsulation of the liquid electrolyte appears as a promising strategy, as it can prevent the leakage of the liquid electrolyte and also provide better transport properties than conventional solid electrolytes. Such composite materials, generally known as gel-polymer electrolytes, have raised considerable attention due to their high versatility, flexibility, and good interfacial contact with the electrode materials. Different polymer matrices have been proposed, including poly(ethylene oxide), poly(methyl methacrylate), poly(acrylonitrile), poly(vinylidene fluoride), or co-polymers of these systems.^[21] Among these candidates, polymethacrylates are widely available, non-toxic, and display a good thermal stability. Moreover, they present a good compatibility with lithium salts and derived electrolytes, offering a wide electrochemical stability window (ESW). The main challenge of poly(methyl methacrylate)hosts lies on their poor mechanical strength. In this regard, P. Isken et al. demonstrated the successful in-situ UV-induced polymerization of methyl ether methacrylate (OEGMA) and benzyl methacrylate (BnMA).^[22] This co-polymer is able to interact with the liquid electrolyte through the ethylene glycol side chains, preventing electrolyte losses, while the BnMA units enhance its mechanical strength. Further research demonstrated promising performances for this polymer host for different energy storage devices, ranging from K-ion batteries to Li-ion capacitors.^[23–26]

Considering the aforementioned, in this work we first propose the formulation of a novel gel-polymer-based electrolyte consisting of a combination of a glyoxylic-acetal-based liquid electrolyte (1 M LiTFSI in TEG:PC (3:7)) and OEGMA:BnMA polymer host. This strategy aims to greatly enhance the safety of the devices by simultaneously employing a less flammable solvent blend and embedding it into a polymer matrix. The physicochemical characteristics and electrochemical performance of this novel GPE are evaluated and compared to its liquid counterpart (1 M LiTFSI in TEG:PC (3:7)). The results show that this GPE provides a good thermal stability and ionic conductivity (1.5 mS cm^{-1}), a wide ESW, as well as similar capacity and cycling stability in LIB cells with lithium iron phosphate (LFP) and hard carbon electrodes.

Experimental

Liquid Electrolyte Preparation

1,1,2,2-tetraethoxyethane (TEG) was supplied by *WeylChem*. To reduce its water content below 20 ppm, the solvent was filtered over dried aluminum oxide (90 active basic, *Merck*) under argon atmosphere. Propylene carbonate (PC; anhydrous 99.7%, *Sigma Aldrich*) was used without further purification. Both solvents were mixed inside an argon filled glovebox in a mass ratio of 3:7. The mixture was used to dissolve 1 M lithium bis(trifluoromethansulfonyl)imide (LiTFSI; 99.9%, *Solvionic*).

Polymer Matrix and Gel-Polymer Electrolyte Preparation

For the preparation of the polymer matrix a previously reported method was followed. Briefly, 0.86 mL (0.90 g, 3 mmol) of oligo(ethylene glycol) methyl ether methacrylate (300 g mol⁻¹) and 1.52 mL (1.59 g, 9 mmol) of benzyl methacrylate were mixed with 4.98 mg (0.2 wt%) of benzophenone. The formulation was placed between two siliconized PET foils and polymerized for 1 h by UV-irradiation (film thickness was adjusted with a spacer of ~200 µm). The polymer films were punched out with a diameter of 12 mm and dried overnight in a Büchi oven at 120 °C. Subsequently, the dried polymer films were transferred to an argon-filled glove box. The gel-polymer electrolyte (GPE) was obtained by swelling the polymer matrix with four times the mass of the liquid electrolyte (1 M LiTFSI in TEG:PC (3:7)) for at least 24 h.

Physicochemical Characterization

Thermogravimetric analysis (TGA) of the liquid electrolyte was conducted using a *Perkin Elmer STA 6000* with nitrogen as the carrier gas at a flow rate of 20 mL min⁻¹ and a heating rate of 10 K min⁻¹. TGA of the polymer matrix and the GPE was measured on a *Netsch TG 209 F1 Libra* under a nitrogen atmosphere with a heating rate of 20 K min⁻¹.

The conductivity of the electrolytes was calculated from the alternating current resistance, obtained from electrochemical impedance measurement. In case of the liquid electrolyte, 500 µL were added into a sealed cell consisting of two perfectly parallel platinized platinum electrodes with a known cell constant (around 1 cm⁻¹, examined with KCl solution). This cell was placed into a climate chamber (*Binder*) and polarized with a voltage of 5 mV at various frequencies ranging from 100 MHz to 100 mHz using a ModulabXM ECS potentiostat (*Solartron Metrology*) at temperatures between -20 and 60 °C. The GPE was placed in a two-electrode *Swagelok* cell with stainless steel electrodes. The thickness of the GPE was measured with a digital caliper gauge by subtracting the length of the empty cell stack from the value with the GPE film. The cell was placed into the climate chamber and the impedance was measured from 1 MHz to 10 Hz with a voltage amplitude of 20 mV using a *BioLogic VSP* potentiostat.

Furthermore, the flash point of the GPE has been investigated using a *Normalab NPV 310* flash point tester operating in an equilibrium closed cup method. In this measurement, the sample is heated with a heating rate of 6 °C per minute and the flammability is tested in intervals of 10 s.

Electrochemical Characterization

The electrochemical stability window of LE and GPE was examined by linear sweep voltammetry in 3-electrode *Swagelok* cells. A 12 mm platinum disk was used as working electrode, an oversized, self-standing activated carbon electrode (85% YP-50 (*Kuraray*), 10% Super C65 (*Imerys*) and 5% Poly(tetrafluorethylen) (*Sigma Aldrich*)) was used as counter electrode and a silver wire served as the reference electrode. The cell was filled with a 13 mm disk of GPE or a 13 mm disk of glass-fiber separator (GF/D, *Whatman*), soaked with 150 µL of LE and polarized with a scan rate of 1 mV s⁻¹ using a *BioLogic VMP-3* potentiostat.

For electrode preparation, 90% of active material (lithium iron phosphate (LFP; *Südchemie*), or respectively hard carbon (Biocarbontron-5 µm, *Kuraray*)) were mixed with 5% of Super C65 (*Imerys*) and an aqueous CMC-SBR binder solution (total share within the slurry: 3,75% Carboxymethylcellulose (CMC; *Walocel CRT2000 GA, Dupont*) and 1.25% Styrene-Butadiene-Rubber (SBR; *Nanografi*) by ball

milling for 3 min, using a *Fritsch Pulverisette 23* high impact ball mill at 50 Hz oscillation frequency. Water-based inks were casted onto Al foil (LFP electrodes) or Cu foil (hard carbon electrodes) respectively, using an *MTI doctor blade*. The resulting film was dried under air atmosphere for 24 h and cut into discs of 12 mm in diameter. The electrode discs were dried under vacuum at 60 °C for 6 h, weighted, and transferred into an argon filled glovebox (*Mbraun*, O₂ and H₂O < 1 ppm).

Electrochemical measurements were conducted using three-electrode *Swagelok* cells. The cells were assembled inside the glovebox, with lithium metal serving as the reference electrode. In the case of the half-cells, lithium metal was simultaneously used as the counter and reference electrode. In cells with LE, a glass-fiber separator (GF/D, *Whatman*) was soaked with 120 µL of 1 M LiTFSI in TEG:PC (3:7). For electrochemical characterization of the GPE, a disk of 13 mm diameter was punched from the Polymer swollen with 1 M LiTFSI in TEG:PC (3:7) and used instead of a glass-fiber separator.

LFP half-cells were galvanostatically charged and discharged within a voltage range of 3.0–3.8 V vs Li/Li⁺ using an *Arbin Instruments LBT21084* Potentiostat. The half-cells containing hard carbon underwent an SEI formation protocol to eliminate the irreversible capacity in the initial cycles. In this protocol, the cell is discharged at a rate of 0.05 C (1 C: 372 mA g⁻¹) for 3 h, followed by discharging to 0.05 V vs. Li/Li⁺ at a rate of 0.1 C. The cell is then charged at a rate of 0.1 C, discharged at a rate of 0.025 C, and finally recharged at a rate of 0.1 C. The cut-off potentials for these three steps are 0.05 V and 2.5 V vs Li/Li⁺. Subsequently, the cells were cycled in a potential range of 0.005–2 V vs. Li/Li⁺ at rates of 0.1, 0.5, and 1 C. Full-cells were assembled using a mass balancing factor of 1:1.7 (HC:LFP) and the SEI formation protocol was applied to the hard carbon electrodes inside half-cells prior to full cell assembly. Galvanostatic charge and discharge measurements of full cells were performed using a *BioLogic VMP-3* or *BioLogic MPG2* Potentiostat. The potential range of the individual electrodes was controlled to 0.005–2 V vs Li/Li⁺ for Hard Carbon and 2.5–3.8 V vs Li/Li⁺ for LFP and the limits for the cell voltage were defined to be 1.5–3.7 V. Potentiostatic electrochemical impedance spectroscopy (PEIS) measurements of the lithium-ion battery full cells were carried out at a frequency range of 200 MHz to 100 mHz using a potential amplitude of 5 mV. The current density and capacity values reported for the half-cells are calculated based on the total mass of active material in the electrodes. For the full-cells, the current density was based on the capacity of the hard carbon electrode. The specific capacity was calculated according to the total mass of both electrodes.

The transference number of lithium ions (t_{Li^+}) in the GPE was determined as described by Sørensen and Jacobsen,^[27] performing PEIS on symmetric Li–Li cells in a frequency range between 100 kHz and 10 µHz, using a excitation amplitude of 10 mV. Scribner ZView software was used to evaluate the spectra and derive the electrolyte resistance (R_E) and the impedance at low frequency due to Warburg diffusion ($Z(0)_d$), which were used to calculate t_{Li^+} according to the following equation:

$$t_+ = \frac{1}{1 + Z(0)_d / R_E}$$

The equivalent circuit model is presented alongside the results in the Figure S1 (Supporting Information).

Scanning Electron Microscopy (SEM) and Energy Dispersive X-Ray Spectroscopy (EDX)

After electrochemical characterization, the used electrodes were analyzed by SEM and EDX. To preserve the compounds formed on the surface, the electrodes were not washed. SEM imaging was performed on a Sigma VP Field Emission Scanning Electron Microscope (Carl-Zeiss AG, Germany) using the InLens/SE detector with an accelerating voltage of 6/10 kV. An Oxford EDX system in combination with a Sigma VP Field Emission Scanning Electron Microscope (Carl-Zeiss AG, Germany) to was used for EDX analysis. The elemental mapping was performed with an acceleration voltage of 15 kV.

Results and Discussion

To better classify the properties of the investigated gel polymer electrolyte (GPE), the following characterization is carried out in comparison with the respective liquid electrolyte (LE). Figure 1 shows the physicochemical properties of both electrolyte systems. As can be expected, the GPE is less ionically conductive compared to LE for all investigated temperatures from –30 °C to 80 °C (Figure 1a). Nevertheless, the conductivity value measured for GPE (1.5 mS cm⁻¹ at 20 °C) is still in the range or even exceeds those measured for liquid electrolytes.^[8] Moreover, its conductivity is superior to the vast majority of previously reported GPEs.^[28–30] Comparing the ionic conductivities of GPE and LE (3.5 mS cm⁻¹) at 20 °C, it is furthermore worth mentioning that the difference between them is only 2 mS cm⁻¹ and thus rather small. A gel-polymer electrolyte consisting of the identical OEGMA:BnMA copolymer matrix and 1 M LiPF₆ in EC:DMC (1:1) reaches around 1.8 mS cm⁻¹ while its liquid counterpart displays a high ionic conductivity of 10.6 mS cm⁻¹ (at 25 °C).^[22,31] This indicates a suitable interaction of the solid and liquid components of the GPE used in the current study.

The thermogravimetric analysis (TGA) underlines the high thermal stability of the TEG:PC electrolyte solvents. For comparison, an electrolyte based on dimethyl carbonate (DMC) as representative for linear carbonate solvents is also shown in Figure 1b.^[14] In the TEG:PC-based electrolyte, major evaporation (>5% mass loss) takes place only at temperatures higher than 97 °C in the dynamic measurement. This stability can even be increased, when confining the liquid inside the OEGMA:BnMA copolymer matrix: The blue curve in Figure 1b, representing the GPE reflects a slight retardation of the evaporation of the liquid electrolyte. Also, it is noteworthy that polymer itself (black curve Figure 1b) displays a thermal stability of 269 °C (5% mass loss).

To further analyze the impact of the OEGMA:BnMA copolymer matrix on the safety characteristics of the electrolyte, the flash point of the GPE has been measured. Compared to the flash point of the LE, which is 96 °C, the GPE presents a notably increased flash point of 127 °C. This underlines the suitability of GPE for the development of safe cell concepts.

The comparatively high thermal stability of pure TEG is accompanied by a moderate electrochemical stability towards high potentials, as it is the case for many ethers.^[32] With 1 M LiTFSI as conductive salt and TEG as single solvent an anodic

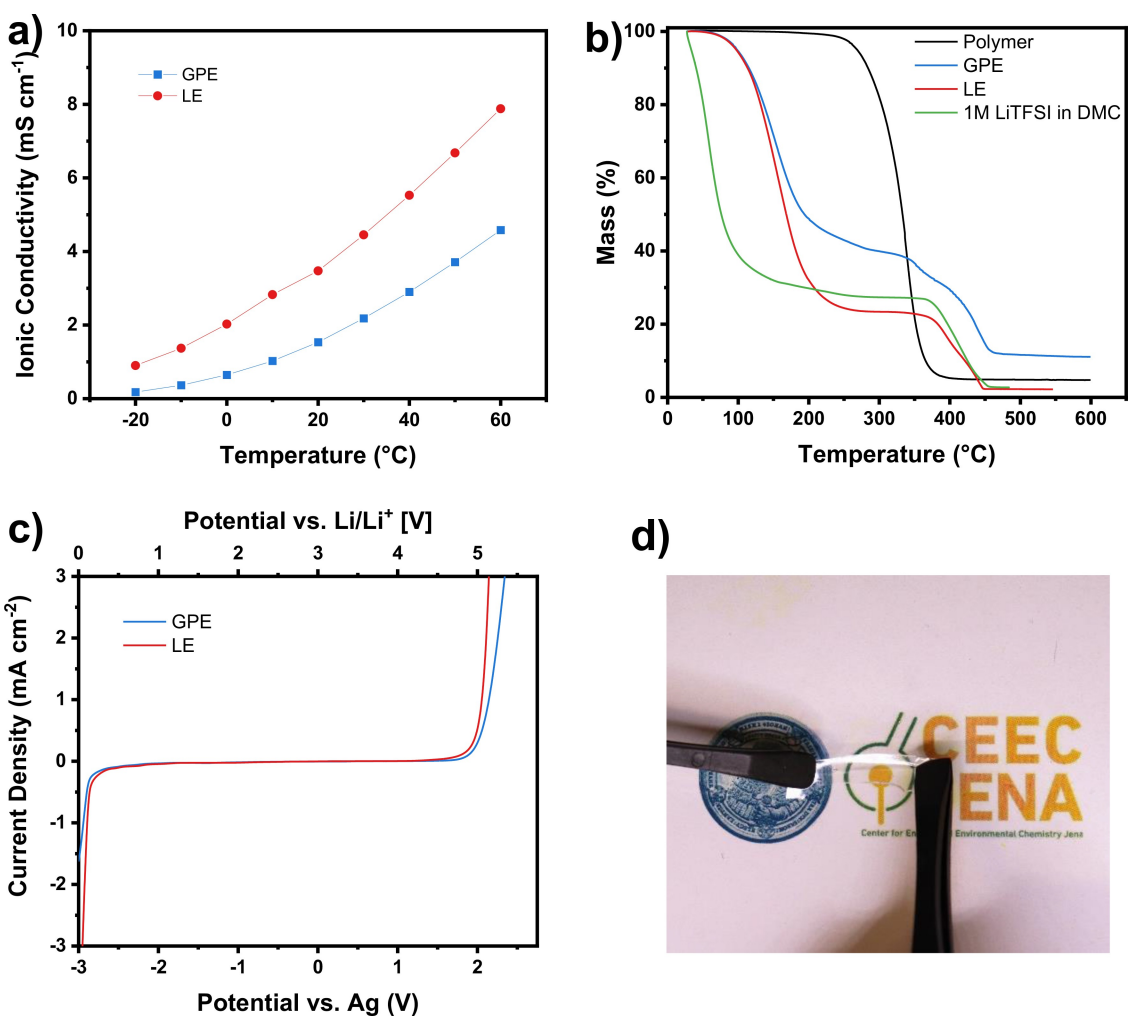


Figure 1. (a) ionic conductivity, (b) thermogravimetric analysis, (c) electrochemical stability window of GPE and LE, (d) image of a piece of GPE.

stability of 4.2 V vs. Li/Li^{+} is obtained. Purely carbonate-based electrolytes, in comparison, can operate at potentials around 5.6 V vs. Li/Li^{+} .^[33] Research works on blends of ether solvents, carbonates, and additives, however, show that the solvation sheath of lithium ions can be modified by adjusting the composition of the solvent mixture, leading to an increase in anodic stability.^[34] In this work, PC is used as co-solvent, which results in an increased ESW compared to purely TEG-based electrolytes. The anodic stability of the GPE electrolyte is around 4.7 V vs. Li/Li^{+} . As can be seen from Figure 1c, the polymer matrix therefore seems to have a positive impact on the stability, as the oxidation onset potential in case of the LE is slightly lower.

Electrochemical Characterization of GPE and LE in LFP Half-Cells

For this comparative work, LFP was chosen as material for the positive electrode, due to the recently increased technical interest for this material,^[35] as well as due to its robustness and easy processability. The LFP electrodes were evaluated in a half-

cell configuration with GPE, and for the purpose of establishing a comparative baseline, the same evaluation was conducted with LE (Figure 2a). A maximum capacity of 137 mAh g^{-1} is obtained when using the GPE, while the LE shows a slightly higher capacity of 143 mAh g^{-1} at 0.1 C. It is worth mentioning that the capacity increases during the first cycles recorded at 0.1 C. This may be associated with an activation process of the material or prolonged wetting. Over additional 170 cycles at 0.5 C (Figure 2b), both electrolyte systems display a coulombic efficiency above 99% and a retention of the initial capacity of more than 89%. Generally, the capacity values with GPE are slightly lower. The reason for this difference can be accessed from the potential profiles in Figure 2c and 2d: A comparison of potentials of the charge and discharge plateaus reveals increased overpotentials associated with the GPE. Additionally, increased sloping can be seen at 0.5 C and 1 C. Nevertheless, the GPE can provide good capacity values at lower C-rates as well as a good capacity retention.

A comparison with literature shows that the capacities obtained for GPE presented in this work at rates between 0.1 C and 1 C are competitive to other methacrylate based GPEs: A bisphenol A ethoxylate dimethacrylate (BEMA) - Poly(ethylene

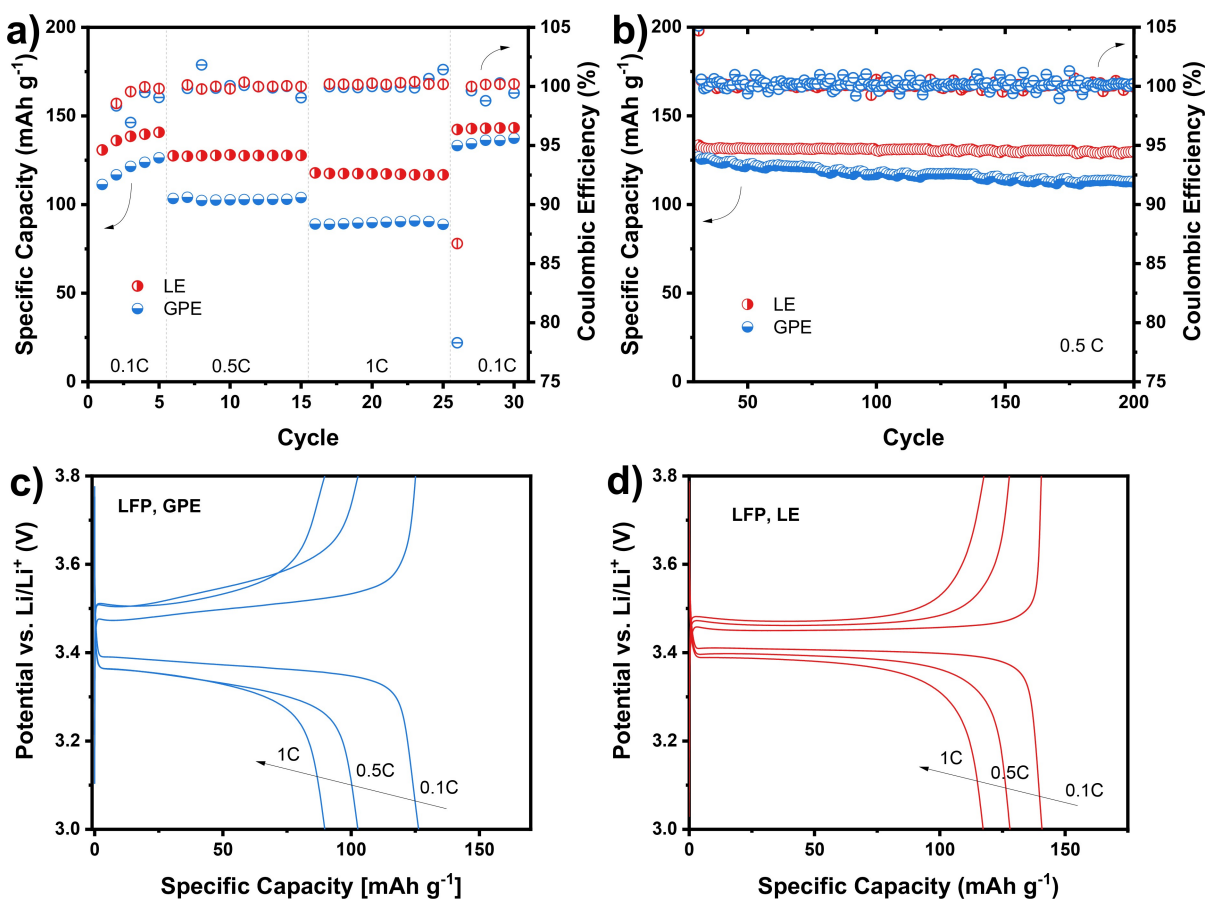


Figure 2. GPE and LE in LFP half-cells: (a) galvanostatic cycling at 0.1 C, 0.5 C, and 1 C (rate capability), (b) galvanostatic cycling at 0.5 C over 170 cycles, (c) potential profiles with GPE, (d) potential profiles with LE.

glycol) methyl ether methacrylate (PEGMA) copolymer soaked with 1.0 M LiPF₆ in EC/DEC (1:1 w/w), introduced by Gerbaldi et al., for example, was capable of providing 125 mAh g⁻¹ at 0.1 C and 98 mAh g⁻¹ at 1 C in LFP half cells.^[36] More recently, Yuan et al. presented a PMMA based composite polymer that was blended with PEO and subsequently combined with 1 M LiClO₄ in EC:PC (1:1).^[37] In half cells with LFP, this GPE showed an advanced rate capability, providing almost 140 mAh g⁻¹ at 1 C. However, the coulombic efficiency of the cells was only around 95% leading to capacity loss over prolonged cycling. However, it should be noted that the works presented in the literature predominantly use LiPF₆ as conductive salt and contain flammable linear carbonates.^[38–42] Although GPEs prevent cell leakage, the flammable solvents and the toxic compounds formed from hydrolysis of LiPF₆ can still represent a safety hazard, if the cells are recycled.^[43]

Electrochemical Characterization of GPE and LE in Hard Carbon Half-Cells

Previous studies on the use of glyoxylic-acetal-based electrolytes in combination with amorphous carbon materials showed that hard carbon is a suitable choice for application at room temperature and even at elevated temperature of 60 °C.^[15] For

this reason, hard carbon was selected as material for the negative electrode. The capacity for this material obtained with the GPE is 232 mAh g⁻¹ at 0.1 C, compared to 258 mAh g⁻¹ for the LE (cycle 1, Figure 3a). Also, the GPE displays an inferior rate capability. By increasing the current density to 1 C (cycle 16, Figure 3a), the capacity provided with the GPE is 47% of the initial value while the LE provides a capacity retention of 67% under the same conditions. Despite the capacity being lower in its absolute value, a good capacity retention of 97% over 170 cycles at 0.5 C was observed for the GPE (Figure 3b). In this case, the capacity retention with the GPE is even higher compared to the LE (88%). In order to gain an understanding of the lower capacity and rate capability observed with GPE, two points may be considered: Firstly, in hard carbons, a large portion of the capacity can be found at low potentials close to 0 V vs. Li/Li⁺. An increase in electrolyte resistance or charge transfer resistance would therefore lead to a loss of capacity. A more detailed consideration of the resistances observed with the two electrolytes will be presented in the discussion of the lithium-ion battery full cells. Secondly, the GPE displays a lower ionic conductivity, which may be relevant at high current densities.

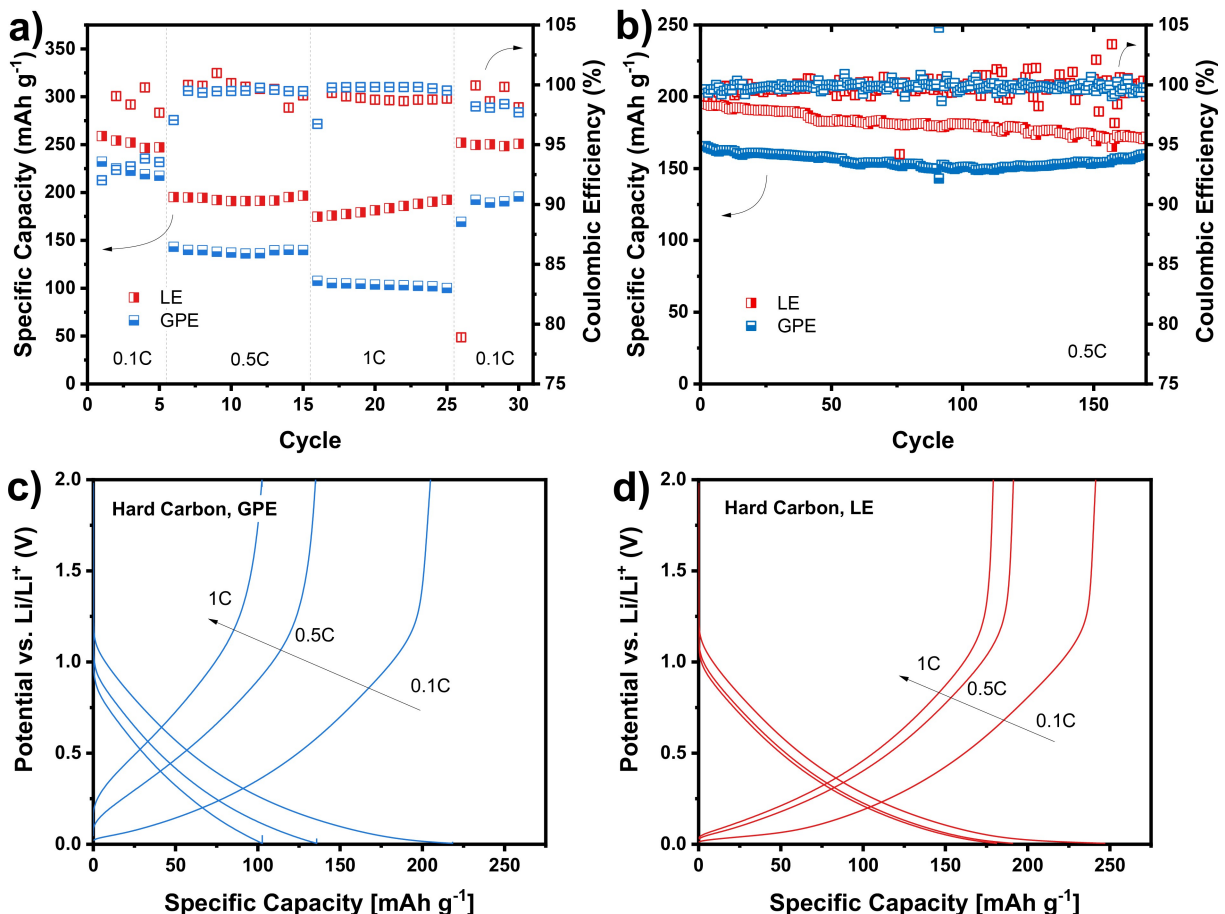


Figure 3. GPE and LE in hard carbon half-cells: (a) galvanostatic cycling at 0.1 C, 0.5 C and 1 C (rate capability), (b) galvanostatic cycling at 0.5 C over 170 cycles, (c) Potential profiles with GPE, (d) potential profiles with LE.

Electrochemical Characterization of GPE and LE in Lab-Scale Lithium-Ion Battery

The tests inside half-cells have proven that the OEGMA:BnMA copolymer soaked with 1 M LiTFSI in TEG:PC (3.7) can be combined with LFP and hard carbon, presenting good cycling stabilities. On basis of these results Li-ion battery full cells have been assembled to gain a deeper understanding of the interaction of the electrolyte systems with both electrodes. The full-cells were charged and discharged within a voltage window of 1.5 to 3.8 V. Simultaneously, potential limits were set for the positive (3.0–3.8 V vs. Li/Li⁺) and the negative electrode (0.005–2.0 V vs. Li/Li⁺). As can be seen from Figure 4a, the specific capacities, calculated according to the mass of both electrodes, at 0.1 C are comparable. However, as already observed for the half-cells, the GPE presents a lower rate capability. By increasing the C-rate from 0.1 C to 1 C, the capacity of the cell containing GPE is reduced by 32% while the capacity of the cell containing LE is reduced by 18%. Notably, these differences in rate capability are less pronounced compared to the half-cells discussed before (cf. Figures 2a and 3a). This suggests that the rate capability might also be influenced by the interaction between the electrolyte system and the lithium metal counter

electrode. A detailed investigation towards GPE and lithium metal batteries is however out of the scope of this work.

Regarding the stability of the presented LIB full-cells over 100 cycles at 0.5 C, it can be seen from Figure 4b that the GPE allows high coulombic efficiency values > 99 % and capacity values comparable to the LE. The potential profiles of the full cells are shown in Figure 4c and 4d. Here, the GPE cell exhibits slightly lower onset potentials for the charge storage related redox process in the discharge, which could be caused by higher resistances. For a deeper understanding of the resistances occurring in the use of GPE, electrochemical impedance analysis has been carried out. The impedance spectra in Figure 4e, which were collected prior to the cycling procedure allow some conclusions on the reasons for the observed results in the rate test. Despite the large differences that may appear on the first sight, both spectra can be fitted by the same equivalent circuit shown in Figure 4f. The latter includes 4 main parts: a resistor that represents the resistance of the electrolyte (R_E), two parallel elements representing the surface layer resistance (R_{SL}) and charge transfer resistance (R_{CT}) and a constant phase element associated with capacitive behavior. Figure 4f shows the values for the resistances resulting from the fit. As can be seen, the full cell containing the GPE possesses a higher R_E , as it also exhibits a lower ionic conductivity (cf.

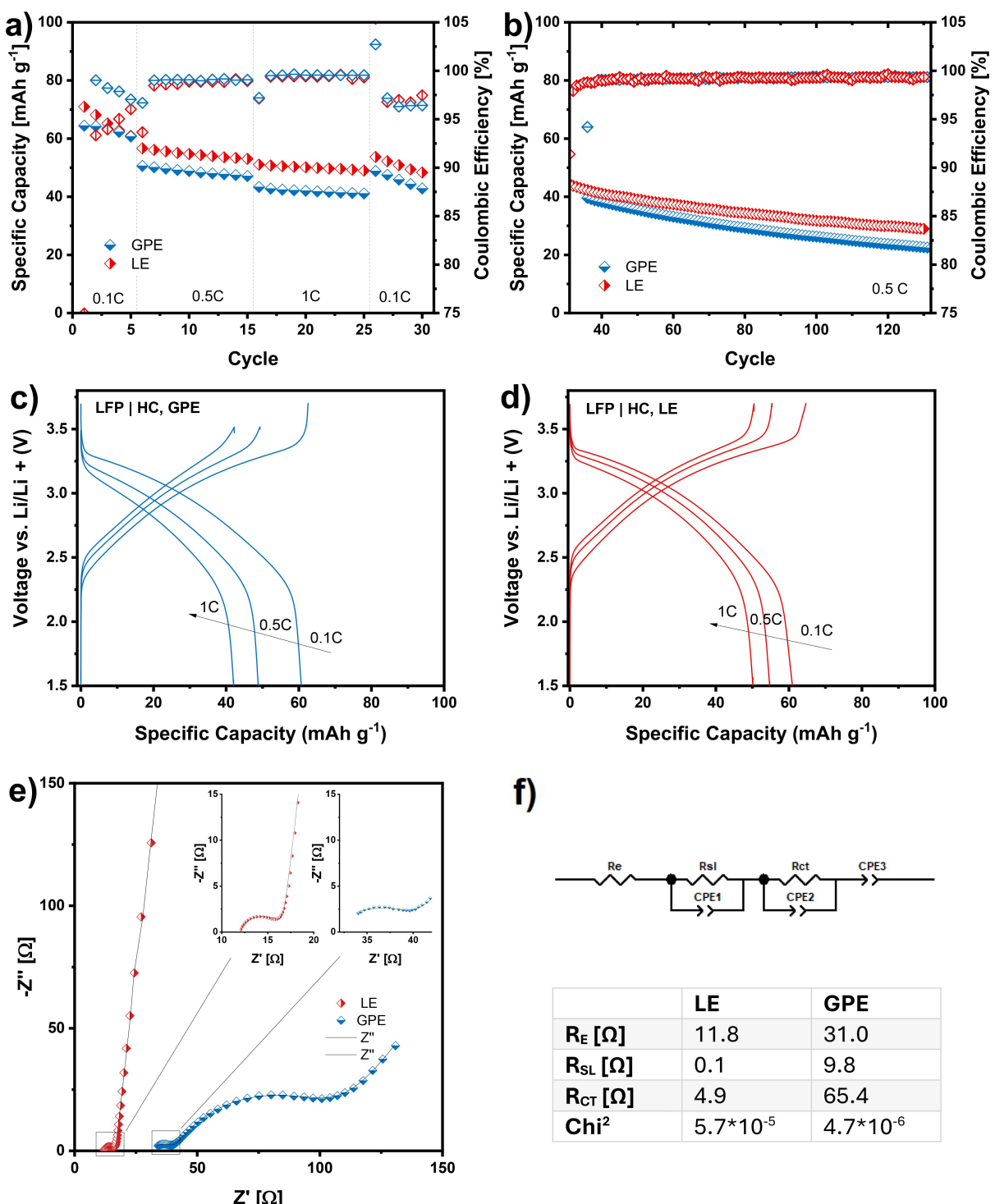


Figure 4. GPE and LE in LIB cells with LFP and hard carbon: (a) galvanostatic cycling at 0.1 C, 0.5 C, and 1 C (rate capability), (b) galvanostatic cycling at 0.5 C over 100 cycles, (c) potential profiles with GPE, (d) potential profiles with LE, (e) electrochemical impedance after cell assembly, (f) equivalent circuit and resulting resistance values for the impedance spectra presented in (e).

Figure 1a). Additionally, the thickness of the GPE varies between 0.5 and 1 mm, whereas the glass fiber separator that is used in the LE cells is 0.52 mm in width. Hence, the distance between the electrodes in the GPE cells may be larger. Apparently, the GPE causes a higher R_{SL} of 9.8Ω and R_{CT} of 65.4Ω , whereas for

the LE, only one semicircle can be observed, which may be associated to a R_{CT} of 4.9Ω , while the R_{SL} is negligible.

These differences in the resistive contributions to the impedance of the full cells, which were mentioned as overpotentials in the discussion of half-cell results, cause the deviation in terms of capacity, when increasing the C-rate.

However, it shall be mentioned that the performance of the GPE does not strongly differ from the LE. Additionally, it would need to be evaluated, how these observations in the tests conducted on lab-scale using *Swagelok* cells, do translate into larger scale production. Especially in the assembly of full cells, it became evident that besides the balancing of the electrodes, the pressure that is applied to the cell on the WE-CE axis, is crucial for the operation of the cell. Figure S2 shows a comparison between a full cell that has been pressed using a screw clamp and another cell that has not been pressed. It becomes evident that a compression of electrodes and GPE can significantly enhance the performance by improving the contact between the porous electrode surface and the gel polymer. Hence, the upscaling into an industrial assembly process with larger cell formats and the optimization process connected to this may lead to improvements on the rate capability of gel-polymer electrolytes.

To evaluate whether the use of GPE has an impact on the surface properties of the electrodes, such as surface layer homogeneity, the electrodes used for the measurements represented in Figure 4 were post-mortem analyzed by EDX. Figure 5a shows the LFP electrodes cycled with GPE on the left side and cycled with LE on the right side. The SEM images visualize the surface of the electrodes, which contain some remaining GPE, or respectively glass-fiber separator in case of LE. The elemental composition of the electrode surface

obtained from EDX does not reflect significant differences between the two electrolytes. Similar contents of carbon, oxygen, iron, sulfur, and phosphorous are detected with a homogeneous distribution. Analogous conclusions can be drawn for hard carbon in Figure 5b. The analysis does not reveal variations in terms of elemental distribution. In contrast to the cathode, fluorine is detected on the anode side, which can be assigned to the SEI layer on the electrode surface. In conclusion, the results from the post-mortem analysis suggest that the GPE does not affect the formation and composition of the interphases.

Conclusions

In this study we combined two approaches addressing the safety characteristics of the electrolyte system in lithium-ion batteries: The use of a less flammable solvent blend containing the glyoxylic-acetal TEG for the liquid electrolyte and the enclosure of the latter into a methacrylate-based polymer matrix. By this strategy, battery leakage can be prevented, while simultaneously increasing the onset temperature of a thermal runaway. Conductivity measurements show that the ionic conductivity of the gel-polymer electrolyte (GPE) is in the same range as the ionic conductivity of the respective liquid electrolyte (LE). The GPE was characterized towards its applicability in

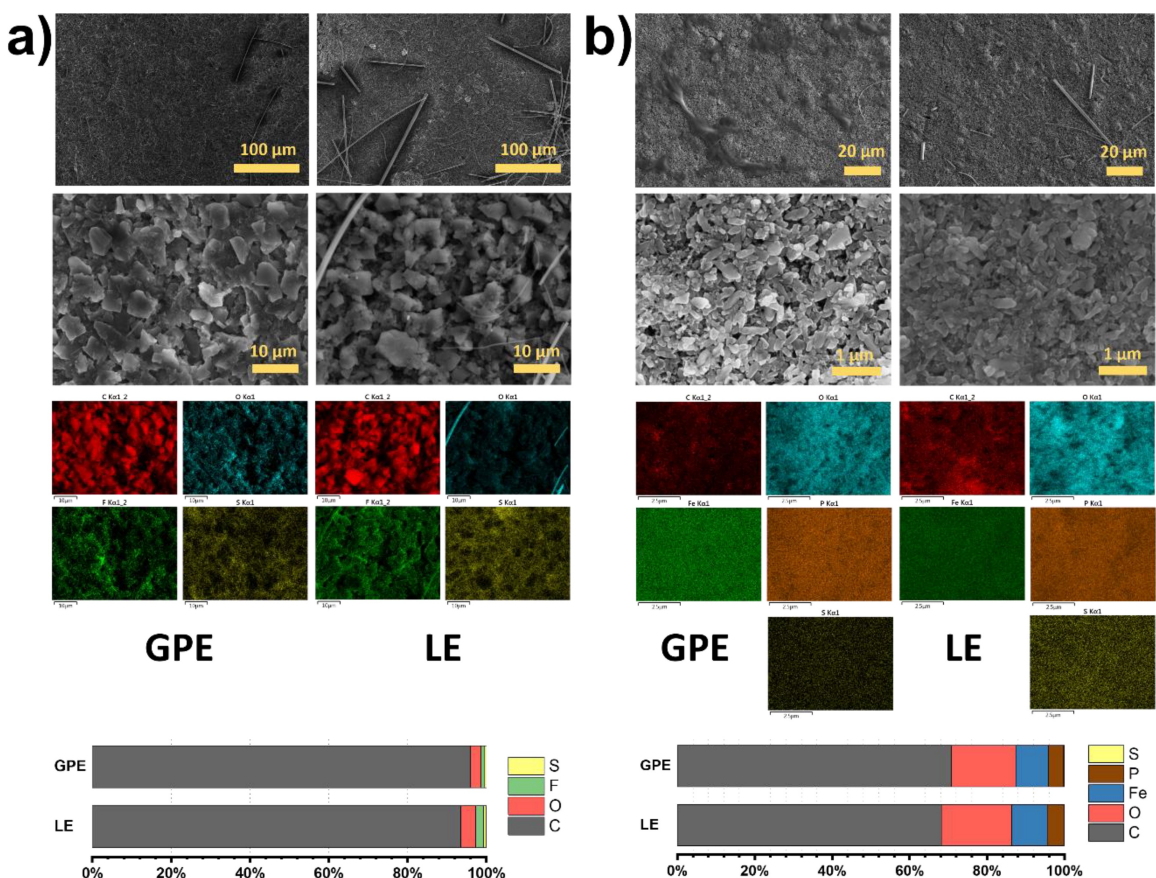


Figure 5. Post-mortem SEM and EDX of (a) hard carbon electrodes, and (b) LFP electrodes cycled the in lithium-ion battery cells presented in Figure 4, cycled with GPE on the left side and cycled with LE on the left side for both electrodes.

lithium-ion batteries comparatively to the LE. From galvanostatic cycling of LFP and hard carbon half-cells, as well as lithium-ion battery full cells containing these two materials, a comparable cycling stability with the two electrolyte systems can be concluded. Although the lithium-ion battery cells with GPE in this experimental setup have a higher electrolyte and charge transfer resistance on a laboratory scale, the results show that gel polymer electrolytes based on low-flammability solvents are a safer alternative to liquid electrolyte systems.

Acknowledgements

The SEM/EDX facilities of the Jena Center for Soft Matter (JCSM) were established with a grant from the German Research Council (DFG). A.B. and J.L.G.U are grateful for the financial support of the European Union's Horizon Europe transport program under the project SiGNE (Grant Agreement No 101069738). C.L. wishes to thank the Carl-Zeiss-Stiftung (CZS) for financial support within the project "Intelligente Substrate: Schaltbare Grenzflächen auf Basis multiresponsiver Hybridmaterialien". Open Access funding enabled and organized by Projekt DEAL.

Conflict of Interests

The authors declare no conflict of interest.

Data Availability Statement

The data that support the findings of this study are available from the corresponding author upon reasonable request.

Keywords: Glyoxal · Glyoxylic-acetal · Gel-polymer electrolyte · Lithium-ion battery

- [1] S. Chen, J. Xiong, Y. Qiu, Y. Zhao, S. Chen, *J. Storage Mater.* **2023**, *63*, 107109.
- [2] Web of Science, Analyze Results: Lithium-ion Batteries (Topic), **2024** (accessed 27.05.2024).
- [3] J. Xu, X. Cai, S. Cai, Y. Shao, C. Hu, S. Lu, S. Ding, *Energy Environ. Mater.* **2023**, *6*, e12450.
- [4] J. Duan, X. Tang, H. Dai, Y. Yang, W. Wu, X. Wei, Y. Huang, *Electrochim. Energy Rev.* **2020**, *3*, 1–42.
- [5] Q. Wang, B. Mao, S. I. Stoliarov, J. Sun, *Prog. Energy Combust. Sci.* **2019**, *73*, 95–131.
- [6] C. Cao, Y. Zhong, Z. Shao, *Chin. J. Chem.* **2023**, *41*, 1119–1141.
- [7] X. Tian, Y. Yi, B. Fang, P. Yang, T. Wang, P. Liu, L. Qu, M. Li, S. Zhang, *Chem. Mater.* **2020**, *32*, 9821–9848.
- [8] F. A. Kreth, L. Köps, C. Leibing, S. Darlami Magar, M. Hermesdorf, K. Schutjajew, C. Neumann, D. Leistenschneider, A. Turchanin, M. Oschatz, J. L. Gómez Urbano, A. Balducci, *Adv. Energy Mater.* **2024**, *14*, 2303909.
- [9] K. S. Teoh, M. Melchiorre, S. Darlami Magar, M. Hermesdorf, D. Leistenschneider, M. Oschatz, F. Ruffo, J. L. Gómez Urbano, A. Balducci, *Adv. Mater.* **2024**, *36*, 2310056.
- [10] G. Hernández, R. Mogensen, R. Younesi, J. Mindemark, *Batteries & Supercaps* **2022**, *5*, e202100373.
- [11] X. Ma, D. Zhang, J. Wen, L. Fan, A. M. Rao, B. Lu, *Chem. A Eur. J.* **2024**, *n/a*, e202400332.
- [12] J. M. Bernard, A. Jomier (Rhodia Operations, Fr.), FR2914310A1, **2008**.
- [13] L. H. Heß, A. Balducci, *ChemSusChem* **2018**, *11*, 1919–1926.
- [14] L. H. Hess, S. Wankmüller, L. Köps, A. Bothe, A. Balducci, *Batteries & Supercaps* **2019**, *2*, 852–857.
- [15] C. Leibing, A. Balducci, *J. Electrochim. Soc.* **2021**, *168*, 090533.
- [16] C. Leibing, D. Leistenschneider, C. Neumann, M. Oschatz, A. Turchanin, A. Balducci, *ChemSusChem* **2023**, *16*, e202300161.
- [17] S. Liu, L. C. Meyer, L. Medenbach, A. Balducci, *Energy Storage Mater.* **2022**, *47*, 534–541.
- [18] M. Klein, M. Binder, M. Koželj, A. Pierini, T. Gouveia, T. Diemant, A. Schür, S. Brutt, E. Bodo, D. Bresser, J. L. Gómez-Urbano, A. Balducci, *Small* **2024**, *20*, 2401610.
- [19] J. Atik, S. Röser, R. Wagner, D. Berghus, M. Winter, I. Cekic-Laskovic, *J. Electrochim. Soc.* **2020**, *167*, 040509.
- [20] L. Köps, C. Leibing, L. H. Hess, A. Balducci, *J. Electrochim. Soc.* **2021**, *168*, 010513.
- [21] M. Zhu, J. Wu, Y. Wang, M. Song, L. Long, S. H. Siyal, X. Yang, G. Sui, *J. Energy Chem.* **2019**, *37*, 126–142.
- [22] P. Isken, M. Winter, S. Passerini, A. Lex-Balducci, *J. Power Sources* **2013**, *225*, 157–162.
- [23] B. Babu, M. Enke, S. Prykhodka, A. Lex-Balducci, U. S. Schubert, A. Balducci, *ChemSusChem* **2021**, *14*, 4836–4845.
- [24] B. Babu, C. Neumann, S. Muench, M. Enke, L. Medenbach, C. Leibing, A. Lex-Balducci, A. Turchanin, U. S. Schubert, A. Balducci, *Energy Storage Mater.* **2023**, *56*, 342–350.
- [25] B. Babu, C. Neumann, M. Enke, A. Lex-Balducci, A. Turchanin, U. S. Schubert, A. Balducci, *J. Power Sources* **2021**, *496*, 229797.
- [26] M. Schroeder, P. Isken, M. Winter, S. Passerini, A. Lex-Balducci, A. Balducci, *J. Electrochim. Soc.* **2013**, *160*, A1753.
- [27] P. Ravn Sørensen, T. Jacobsen, *Electrochim. Acta* **1982**, *27*, 1671–1675.
- [28] L. Long, S. Wang, M. Xiao, Y. Meng, *J. Mater. Chem. A* **2016**, *4*, 10038–10069.
- [29] R. C. Agrawal, G. P. Pandey, *J. Phys. D* **2008**, *41*, 223001.
- [30] Z. Osman, M. I. Mohd Ghazali, L. Othman, K. B. Md Isa, *Results Phys.* **2012**, *2*, 1–4.
- [31] K. Xu, *Chem. Rev.* **2004**, *104*, 4303–4418.
- [32] K. Xu, *Chem. Rev.* **2014**, *114*, 11503–11618.
- [33] J. Kasnatscheew, B. Streipert, S. Röser, R. Wagner, I. Cekic Laskovic, M. Winter, *Phys. Chem. Chem. Phys.* **2017**, *19*, 16078–16086.
- [34] H. Jia, Y. Xu, S. D. Burton, P. Gao, X. Zhang, B. E. Matthews, M. H. Engelhard, L. Zhong, M. E. Bowden, B. Xiao, K. S. Han, C. Wang, W. Xu, *ACS Appl. Mater. Interfaces* **2020**, *12*, 54893–54903.
- [35] International Energy Agency (IEA) *Global EV Outlook 2023*, IEA, Paris **2023**.
- [36] C. Gerbaldi, J. R. Nair, G. Meligrana, R. Bongiovanni, S. Bodoardo, N. Penazzi, *J. Appl. Electrochim.* **2009**, *39*, 2199–2207.
- [37] G. Yuan, H. Zhang, M. Wang, X. Chen, H. Guo, X. Chen, *J. Appl. Polym. Sci.* **2021**, *138*, 49799.
- [38] A. Chiappone, J. R. Nair, C. Gerbaldi, L. Jabbour, R. Bongiovanni, E. Zeno, D. Beneventi, N. Penazzi, *J. Power Sources* **2011**, *196*, 10280–10288.
- [39] Y. Huang, B. Liu, H. Cao, Y. Lin, S. Tang, M. Wang, X. Li, *J. Solid State Electrochim.* **2017**, *21*, 2291–2299.
- [40] T. C. Nirmale, I. Karbhal, R. S. Kalubarne, M. V. Shelke, A. J. Varma, B. B. Kale, *ACS Appl. Mater. Interfaces* **2017**, *9*, 34773–34782.
- [41] Q. Wang, X. Xu, B. Hong, M. Bai, J. Li, Z. Zhang, Y. Lai, *Chem. Eng. J.* **2022**, *428*, 131331.
- [42] K. Yang, X. Ma, K. Sun, Y. Liu, F. Chen, *J. Solid State Electrochim.* **2018**, *22*, 441–452.
- [43] A. Sonoc, J. Jeswiet, V. K. Soo, *Proc. CIRP* **2015**, *29*, 752–757.

Manuscript received: July 2, 2024

Revised manuscript received: August 30, 2024

Accepted manuscript online: September 9, 2024

Version of record online: October 29, 2024